Pre-symptomatic development of lower motor neuron connectivity in a mouse model of severe spinal muscular atrophy

HMG Advance Access published November 2, 2009

Pre-symptomatic development of lower motor neuron connectivity in a mouse model of severe spinal muscular atrophy

Lyndsay M. Murray[1,2], Sheena Lee[3], Dirk Bäumer[3], Simon H. Parson[1,2], Kevin Talbot[3] & Thomas H. Gillingwater[1,2]*

[1]Centre for Integrative Physiology & [2]Euan MacDonald Centre for Motor Neuron Disease Research, University of Edinburgh Medical School, Edinburgh, EH8 9XD, UK

[3]MRC Functional Genomics Unit, Department of Physiology, Anatomy and Genetics, University of Oxford, Oxford, OX1 3QX, UK

* Corresponding Author:

Dr Thomas H. Gillingwater
Centre for Integrative Physiology
University of Edinburgh Medical School
Hugh Robson Building
Edinburgh
EH8 9XD
UK
Email: T.Gillingwater@ed.ac.uk
Tel: +44 (0)131 6503724
Fax: N/A

Abstract

The childhood motor neuron disease Spinal Muscular Atrophy (SMA) results from reduced expression of the Survival Motor Neuron (*SMN*) gene. Previous studies using *in vitro* model systems and lower organisms have suggested that low levels of Smn protein disrupt prenatal developmental processes in lower motor neurons, influencing neuronal outgrowth, axon branching and neuromuscular connectivity. The extent to which these developmental pathways contribute to selective vulnerability and pathology in the mammalian neuromuscular system *in vivo* remains unclear. Here, we have investigated pre-symptomatic development of neuromuscular connectivity in differentially vulnerable motor neuron populations in *Smn-/-;SMN2* mice, a model of severe SMA. We show that reduced Smn levels have no detectable effect on morphological correlates of pre-symptomatic development in either vulnerable or stable motor units, indicating that abnormal pre-symptomatic developmental processes are unlikely to be a pre-requisite for subsequent pathological changes to occur *in vivo*. Microarray analyses of spinal cord from two different severe SMA mouse models demonstrated that only minimal changes in gene expression were present in pre-symptomatic mice. In stark contrast, microarray analysis of late-symptomatic spinal cord revealed widespread changes in gene expression, implicating extracellular matrix integrity, growth factor signalling and myelination pathways in SMA pathogenesis. Taken together, these data suggest that reduced Smn levels induce SMA pathology by instigating rapidly progressive neurodegenerative pathways in lower motor neurons around the time of disease onset rather than by modulating pre-symptomatic neurodevelopmental pathways.

Introduction

Proximal autosomal recessive Spinal Muscular Atrophy (SMA) is a devastating childhood form of motor neuron disease, targeting lower motor neurons in the ventral horn of the spinal cord resulting in denervation and atrophy of muscles in the limbs and trunk [1]. It is the most common genetic cause of infant mortality in the human population, with an incidence of around 1:6,000-10,000 [1-3], and is caused by low levels of the survival motor neuron protein (Smn). Smn is the ubiquitously-expressed protein product of a gene which exists in two near identical copies: *SMN1* and *SMN2* [3,4]. Reduced protein levels result from loss or disruption of the telomeric *SMN* gene (*SMN1*) but retention of the centromeric *SMN* gene (*SMN2*). The disease is characterised by an early disruption of neuromuscular connectivity, in the form of functional disruption and structural loss of neuromuscular junctions, which precedes a loss of lower motor neuron soma from the spinal cord and wasting of skeletal muscle [5-9]. Despite a clear understanding of the genetic cause of SMA, our understanding of the cellular and molecular mechanisms through which mutations in *SMN* lead to selective motor neuron loss and resultant clinical symptoms remains incomplete [1].

Several studies have suggested that reduced Smn protein levels can have a significant influence on neurodevelopmental processes in lower motor neurons. For example, results from experiments using cultured neurospheres have shown that neuronal differentiation is inhibited in *Smn-/-;SMN2* cells [10] and *in vitro* experiments utilising *Smn-/-;SMN2* motor neurons reported reduced axon outgrowth [11,12]. Furthermore, axon outgrowth and pathfinding have been shown to be compromised in zebrafish and *Xenopus* models of SMA [13,14]. Although a failure to establish the neuromuscular system during embryogenesis appears unlikely to contribute to any developmental phenotype [15], these studies suggest that deficiencies in motor unit development (controlling factors such as motor unit branching,

size, pruning and function) may play a major role in conferring pre-symptomatic vulnerability upon lower motor neurons. Indeed, these studies have led to the suggestion that SMA may be caused by incorrect development of the neuromuscular system, which would subsequently confer an intrinsic vulnerability upon lower motor neurons pre-symptomatically, during pre-natal stages of growth and maturation. If this model of SMA pathogenesis turns out to be correct, then attempts to rescue the neuromuscular system post-natally (e.g. by elevating levels of Smn protein using gene therapy or pharmaceutical approaches [16,17]) would likely have significant limitations. However, if pre-symptomatic developmental abnormalities are not a major feature of SMA, the neuromuscular system may remain intact until the postnatal onset of symptoms and therefore be more amenable to rescue.

If prenatal developmental processes such as neuronal outgrowth and axon branching significantly contribute to SMA pathogenesis in mammals *in vivo*, we would expect to observe significant changes in the gross and/or fine morphology of neuromuscular connectivity, and/or changes in gene expression patterns in the spinal cord, preceding the onset of neuromuscular pathology in an established mouse model of severe SMA (*Smn-/-;SMN2* [18]). To directly test this, we have undertaken a combined high-resolution analysis of neuromuscular morphology and gene expression in SMA mice at a pre-symptomatic age (postnatal day 1; P1). We have taken advantage of previous observations that different muscles/muscle regions are differentially vulnerable to pre-synaptic pathology [7] and examined pre-symptomatic development in neighbouring populations of lower motor neurons and neuromuscular junctions that are known to be subsequently vulnerable or resistant to pathological changes at later stages of disease progression (P5). We show that morphological perturbations in pre-symptomatic developmental pathways are neither present nor necessary

for subsequent lower motor neuron pathology to occur in SMA *in vivo*. Parallel gene expression analyses of pre-symptomatic spinal cord from *Smn-/-;SMN2* and slightly less severe *Smn-/-;SMN2;delta7* [19] mice confirmed the absence of any disruption of developmental pathways, whereas equivalent microarray analyses at late-symptomatic ages indicated an extensive breakdown in neuronal integrity, implicating extracellular matrix stability, myelination and growth factor signalling pathways in disease pathogenesis.

Results

No detectable morphological abnormalities in pre-symptomatic development in either vulnerable or non-vulnerable motor units in severe SMA mice.

To establish whether pre-symptomatic developmental abnormalities are a significant feature of SMA pathogenesis *in vivo* we initially examined morphological correlates of lower motor neuron connectivity in the *Smn-/-;SMN2* mouse model of severe SMA at pre-symptomatic ages (post-natal day 1; P1 [18,7]). We have previously shown that, in our hands, *Smn-/-;SMN2* mice (as well as less severe *Smn-/-;SMN2;delta7* mice; see below) are indistinguishable from their wild-type littermates at P1 and that pathological changes in the neuromuscular system are almost entirely absent [7; Baumer et al., manuscript under review].

The homogeneously fast-twitch Levator Auris Longus (LAL) muscle provided us with an excellent model system with which to study selectively vulnerable populations of lower motor neurons in these mice, allowing a direct comparison of neighbouring populations of differentially-affected motor units whilst eliminating variables such as nerve stump length, muscle fibre type and muscle function [7]. Whole mount LAL muscles from P1 *Smn-/-;SMN2* and litter-mate control mice (*Smn+/+;SMN2*,) were labelled with antibodies against 150kDa neurofilament to reveal axonal and synaptic morphology and rhodamine-conjugated

α-bungarotoxin to label post-synaptic acetylcholine receptors at the neuromuscular junction [7,20].

Confocal micrograph montages of the whole LAL muscle (incorporating both caudal and rostral bands) allowed analysis of the gross muscle innervation pattern in pre-symptomatic P1 mice (Figure 1). No differences were observed between the gross innervation patterns of either the rostral (non-vulnerable motor units) or caudal (vulnerable motor units) bands of the LAL in *Smn-/-;SMN2* and litter-mate control mice (N=8 control muscles; N=14 *Smn-/-;SMN2* muscles). Endplates were clustered into distinct and highly characteristic innervation bands in all muscles examined: termed C1 and C2 in the caudal band and R1-5 in the rostral band (Figure 1A). Axons entered adjacent to region C1 in all muscles examined and, although there was a small amount of normal biological variability within genotypes, gross intra-muscular nerve branching patterns were not altered in *Smn-/-;SMN2* muscles (Figure 1D). Quantification of the numbers of neuromuscular synapses in regions C2 and R3-5 (selected because these areas were least likely to suffer damage during muscle dissection) revealed no differences between *Smn-/-;SMN2* and control mice (Figure 1E,F). This was in agreement with previous studies that reported no obvious discrepancy in the initial embryonic establishment of neuromuscular innervation patterns in SMA mice [15].

Next, we considered the possibility that pre-symptomatic changes in lower motor neuron branching and motor unit size could conceivably lead to excessive demands being placed on individual lower motor neurons (e.g. functionally and/or energetically), thereby damaging the cell and pre-disposing it to subsequent degeneration. Such defects in axonal pathfinding and/or branching would most likely manifest as alterations in the number of axons present in intramuscular nerve bundles. We therefore quantified axon number in intramuscular nerve

bundles innervating regions C2 and R3 (two anatomically highly-consistent areas of the LAL muscle) in *Smn-/-;SMN2* and control mice (Figure 2). Axons were only quantified in areas of the muscle where the complete endplate band could be seen in order to ensure that no other axon branches were entering the endplate band from a different nerve bundle. We did not observe sensory axons in any of the intramuscular axon bundles investigated (i.e. there were no axon profiles extending beyond the endplate band innervating sensory organs), meaning that all analyses only contained motor axons innervating the endplate region under investigation. Initial attempts to quantify the numbers of individual axons in intramuscular nerve bundles by undertaking analyses on raw confocal stacks and z-projections proved inconsistent and unreliable (Figure 2A&C). To achieve the necessary resolution required for accurate and robust analysis, confocal stacks were subjected to deconvolution analyses (Figure 2B&D). Quantification of axon numbers normalised to the number of endplates innervated revealed no difference in the numbers of axons innervating either C2 or R3/4 regions of *Smn-/-;SMN2* or control mice (Figure 2E).

We next considered the possibility that subtle differences in the terminal branching of lower motor neurons (at the level of axonal inputs to individual neuromuscular junctions) could lead to hyper-innervation of muscle and a corresponding increase in motor unit size pre-symptomatically in SMA. To address this possibility we counted the number of axon collaterals converging on individual post-synaptic endplates at neuromuscular junctions in both bands of the LAL muscle from *Smn-/-;SMN2* and control mice. Note that at this age, neuromuscular junctions are normally poly-neuronally innervated, as the process of developmental synapse elimination is ongoing. No significant differences were found in the average number of inputs converging on endplates in either rostral or caudal bands between genotypes (Figure 3). There was a small, but noticeable, trend towards an increased number

of inputs in *Smn-/-;SMN2* mice compared to controls. However, as this small increase was present in both bands of the LAL, and equivalent levels were also observed in heterozygote controls (data not shown), these small differences are unlikely to contribute to subsequent selective neuromuscular vulnerability in the caudal band of the LAL.

During our analyses of P1 muscles we observed numerous axon sprouts, in the form of neuronal projections extending from pre-synaptic motor nerve terminals (Figure 4), that have not been previously reported in the literature. These 'developmental sprouts' were consistently present in all bands of all muscles analysed, including both *Smn-/-;SMN2* and litter-mate control mice. Developmental sprouts ranged in size from under 5µm to around 250µm. To confirm that this was a natural phenomenon, and that it was not occurring due to the presence of the *SMN2* transgene, we examined P1 muscles from wild-type CD1 mice (a completely unrelated genetic strain). Terminal developmental sprouts were present in CD1 mice and were indistinguishable from those observed in *Smn-/-;SMN2* and control mice at the same age (Supplementary Figure 1). Whilst this finding clearly warrants further investigation in future studies of normal neuromuscular development, it also serves to demonstrate that the 'developmental sprouts' described here are not pathological and are distinct to previously described 'denervation-induced sprouts' which occur as a compensatory response to a loss of synaptic innervation at the neuromuscular junction [21]. However, neither the numbers of small (<150µm; see methods) nor larger 'super sprouts' (those >150µm in length) were modified in pre-symptomatic *Smn-/-;SMN2* mice (Figure 4).

Taken together, these data show that pre-symptomatic development of lower motor neuron connectivity, as far as can be observed using morphological techniques, occurs normally in both vulnerable and non-vulnerable motor units in severe SMA mice.

No detectable morphological abnormalities in post-synaptic maturation in Smn-/-;SMN2 mice

As lower motor neuron morphology and connectivity were unaffected in *Smn-/-;SMN2* mice at pre-symptomatic stages, we next investigated whether changes in post-synaptic development at the neuromuscular junction were present and could account for subsequent vulnerability of motor units. In agreement with previous studies, we have already established that the position and relative number of post-synaptic motor endplates were normal in both caudal and rostral bands of the LAL muscle in *Smn-/-;SMN2* mice (Figure 1E). Quantification of individual endplate areas revealed a similar, normal distribution in *Smn-/-;SMN2* mice (Figure 5C). As previous work has suggested that endplate maturation may have an impact upon lower motor vulnerability in SMA mice [22], we applied a scale to quantify and compare endplate maturation in *Smn-/-;SMN2* and control mice (Figure 5A). Endplates were categorised as either 'uniform', where AChR receptors were evenly distributed within the endplate area, 'folded' where bright bands on the endplate had formed which were indicative of post synaptic fold formation (a sign of early maturation), or perforated, where holes in the AChR labelling were indicative of the endplate beginning to take on the adult 'pretzel-like' morphology [23]. Overall, there was no difference in the numbers or proportion of uniform, folded and perforated endplate morphologies between genotypes (Figure 5B). However, we observed an increase in endplate maturation in the caudal band of the LAL in mice from both genotypes, as evidenced by an increase in the number of folded and perforated endplates. This finding is consistent with motor units in the caudal band conforming to fast-synapsing 'FaSyn' characteristics, being developmentally more advanced than their delayed-synapsing 'DeSyn' neighbours [7,24] (note that FaSyn and DeSyn characteristics of motor units have no relevance to the fast-twitch / slow-twitch phenotype of motor units).

No detectable differences in pre-symptomatic development between differentially vulnerable fast-twitch and slow-twitch muscles

Our finding that there were no detectable abnormalities in the development of lower motor neuron connectivity in both the rostral and caudal bands of the LAL implied that abnormal pre-symptomatic neuromuscular development does not contribute to the increased vulnerability of motor units in the caudal band of the LAL [7]. However, these analyses compared two bands of a homogenous fast-twitch muscle (albeit with different FaSyn/DeSyn characteristics). It therefore remained possible that abnormalities in pre-symptomatic development of lower motor neuron connectivity may contribute to the increased vulnerability of lower motor neurons innervating slow-twitch muscles compared to those innervating fast-twitch muscles [7]. To investigate this possibility, we increased the scope of our experiments to examine two muscles immediately deep to the LAL muscle: abductor auris longus (AAL) and auricularis superior (AS). The AAL is a predominantly fast-twitch muscle whilst the AS is predominantly slow-twitch (Figure 6). We chose these muscles for comparison because of their close proximity and function to one another (and the LAL) as well as their common innervation by the facial nerve (eliminating variables such as nerve stump length and body position, while still allowing whole mount analysis of the complete innervation pattern within a muscle). In late-symptomatic (P5) *Smn-/-;SMN2* mice, there was approximately 25% denervation in the slow-twitch AS muscle while the fast-twitch AAL remained relatively unaffected (Figure 6). The increased vulnerability of slow-twitch muscles at late-symptomatic stages was therefore reflected in the increased pathology observed in the AS muscle.

Comparable analyses of pre-symptomatic development to those detailed above for the LAL muscle revealed no significant differences in gross or fine neuromuscular development in the

AAL or AS muscles between *Smn-/-;SMN2* and control mice (Figure 7). Interestingly, more advanced endplate maturation was observed in the less vulnerable AAL muscle compared to the AS muscle.

Minimal changes in pre-symptomatic gene expression in mouse models of SMA.

The experiments detailed in this study strongly suggest that lower motor neuron connectivity develops normally up until the onset of degenerative symptoms post-natally in severe SMA mice. Despite finding no morphological evidence for abnormal pre-symptomatic development of the neuromuscular system, it remained possible that developmental changes at the level of gene expression could impact on lower motor neuron vulnerability without modifying morphology. To investigate this possibility, we undertook gene expression analyses in pre-symptomatic (P1) *Smn-/-;SMN2* mouse spinal cord (N=4 mice per genotype, littermate matched). We used Affymetrix Mouse Exon ST arrays (see methods for protocol and details concerning experimental controls) to identify any statistically significant genes showing more than 1.5 fold changes in expression levels. Out of 16,755 genes examined at P1, only 3 were significantly changed >1.5 fold (Table 1). The largest change observed was in expression levels of *SMN1*, providing an internal control for the sensitivity of the experiment. The other two genes identified fell close to the margin of the 1.5 fold cut off (1.6 fold down regulation and 1.7 fold up-regulation; Table 1), but neither are considered important for development of the neuromuscular system.

To validate the virtual absence of gene expression changes in the *Smn-/-;SMN2* microarray data, we repeated the microarray experiment using pre-symptomatic (P1) spinal cord tissue from the less severely affected *Smn-/-;SMN2;delta7* mouse model of SMA (N=4 mice per genotype, littermate matched; [19]). These experiments revealed a similar lack of large-scale

expression changes for genes implicated in developmental pathways (Table 2). Taken together, these data suggest that reduced *SMN* expression levels exert no significant effect on pre-symptomatic gene expression in the spinal cord *in vivo*.

Significant changes in gene expression were present in late-symptomatic Smn-/-;SMN2 mice

As our morphological and gene expression analyses of SMA mice demonstrated that modifications in pre-symptomatic developmental pathways are unlikely to impact on subsequent SMA pathogenesis, we concluded that the breakdown of lower motor neurons is more likely due to the instigation of post-natal degenerative pathways. In order to gain insight into the identity of cellular and molecular pathways underlying breakdown of the neuromuscular system in SMA, we repeated our microarray expression analysis using late-symptomatic (P5) spinal cord from *Smn-/-;SMN2* mice (N=3 mice per genotype, littermate matched). Of the 16,755 individual genes investigated, 160 were significantly changed ($P<0.05$, unpaired t test) greater than 1.5 fold (Table 3 shows changes >2 fold; Supplementary Table 1 shows changes >1.5-1.99 fold). No multiple testing correction was applied to the data (e.g. Benjamini and Hochberg) as it was considered to be over-stringent for microarray data of this nature and sample size (i.e. no genes would be expected to pass the test). Array data were therefore validated at the protein level using quantitative western blotting (see below). Both increases and decreases in gene expression levels were observed in *Smn-/-;SMN2* mice, but none of the significantly increased genes were changed greater than 2-fold (therefore genes with increased expression can only to be found in Supplementary Table 1). The biggest single change was found for a gene in the myelination pathway, where we detected a significant 6.5 fold decrease in expression of myelin protein zero (P0). These results were in stark contrast to the P1 results (a 53 fold increase in the number of changed genes), underlining the minimal changes seen pre-symptomatically. A comparison of P1 and

P5 data also clearly underlined the scale and rapid progression of pathological changes that occur in the neuromuscular system in this severe model of SMA.

Utilisation of GO-Elite MAPPFinder software to further investigate the potential function of genes shown to have modified expression levels identified 35 different cellular pathways which were modified in late-symptomatic (P5) *Smn-/-;SMN2* spinal cord (Table 4). This *in silico* analysis highlighted changes in pathways relating to extracellular matrix integrity and growth factor signalling in SMA pathology.

To validate the microarray findings and confirm that changes detected at the mRNA level in spinal cord led to corresponding changes at the protein level, we quantified protein expression levels of myelin protein zero (P0) in the spinal cord of late-symptomatic *Smn-/-;SMN2* mice and wild-type littermates at P5 using fluorescent western blotting (see methods). We observed a significant (~50%) reduction in P0 protein levels in *Smn-/-;SMN2* mice, thereby validating the microarray dataset and confirming that the large reduction in P0 mRNA detected on the microarray resulted in corresponding reductions in protein expression (Figure 8).

Discussion

This study has generated two important findings. First, we have demonstrated that reduced Smn expression does not significantly modify pre-symptomatic lower motor neuron connectivity or gene expression in the spinal cord *in vivo*. Abnormal pre-symptomatic development of lower motor neuron connectivity is therefore unlikely to be a pre-requisite for subsequent pathology to occur in a mouse model of severe SMA. Second, we have shown that gene expression changes correlating with SMA pathology progress rapidly following the onset of symptoms, and that extracellular matrix integrity, growth factor signalling and/or myelination pathways may constitute viable therapeutic targets for stabilising lower motor neuron and spinal cord pathology in SMA. This study therefore highlights the importance of focusing on the role of Smn protein in maintaining the neuromuscular system once formed, rather than its role in regulating motor neuron outgrowth and axonogenesis, for understanding SMA pathogenesis.

Our data suggest that the developmental effects of reduced Smn levels reported *in vitro* as well as in zebra fish and *Xenopus* models *in vivo* [10-14] are not mirrored in mammalian SMA models *in vivo*. Whilst it remains possible that Smn protein can influence developmental pathways including axon outgrowth and pathfinding in mammals under some experimental conditions, our data demonstrate that such changes are not sufficient to cause defects in the development of lower motor neuron connectivity in mouse models *in vivo* and are therefore not likely to be a major contributing factor to SMA pathogenesis in human patients. As a result, efforts to understand the role of Smn protein in the triggering and progression of SMA pathology would likely be better served by focussing on events occurring during and around the onset of symptoms and motor neuron breakdown. Our data also suggest that modifier genes which influence disease severity in SMA, such as plastin 3

[25], are more likely to work through stabilising the neuromuscular system (e.g. by modifying actin dynamics) rather than by influencing pre-symptomatic developmental pathways such as axonogenesis [c.f. 25].

Although we could not detect alterations in pre-symptomatic development of lower motor neuron connectivity *in vivo*, we did observe some subtle differences between neuromuscular development of the rostral and caudal bands of the LAL, and between the AS and AAL muscles. The finding that endplate maturation was occurring faster in the caudal band of the LAL muscle is in agreement with our previous findings that motor units in this muscle band belong to the developmentally more advanced fast-synapsing ('FaSyn') subtype [7,24]. Whilst this may indicate that increased maturation is linked to increased vulnerability, advanced endplate maturation was also seen in the relatively non-vulnerable AAL muscle compared to the less mature endplates in the vulnerable AS muscle. These results indicate that the rate of endplate maturation is unlikely to directly impact upon motor unit vulnerability in SMA. This is in contrast to recent published findings suggesting that increasing endplate maturation by exercise stabilises the neuromuscular junction and confers neuroprotection [22]. In light of our findings we would suggest revising the conclusions of Biondi and colleagues [22] to state that, while exercise can clearly be neuroprotective in SMA, endplate maturation is probably a by-product of the exercise regime and is not likely to have a direct effect on lower motor neuron vulnerability.

One remarkable finding of the current study was that pre-symptomatic analyses of lower motor neuron morphology and gene expression revealed no detectable abnormalities in pre-symptomatic development of lower motor neuron connectivity at P1, in a severe mouse model of SMA where the disease kills the animals by P6-P7. This highlights the rapid

progression of neuromuscular breakdown that occurs as a result of reduced *SMN* expression, but also gives great encouragement for the development of post-natally delivered treatments for SMA in human patients. Had we found evidence for widespread disruption of pre-symptomatic development of lower motor neurons, leading to subsequent changes in neuronal vulnerability, it would be difficult to envisage how this could be fully remedied by post-natal treatment options alone. By contrast, our results suggest the potential existence of a pre-symptomatic "therapeutic time window" in which the majority of lower motor neurons and neuromuscular synaptic connections remain phenotypicaly intact, extending into post-natal days even in a mouse model of severe SMA where death occurs by P5-P6. This work therefore provides encouragement for current efforts to treat SMA post-natally, using strategies such as increasing *SMN* levels in the nervous system [16,26] or increasing full-length splicing from the preserved *SMN2* gene [17,27-33].

Our finding that pre-symptomatic developmental pathways are unlikely to contribute significantly to SMA pathogenesis suggests that a focus on cellular and molecular pathways active around the time of symptom onset will be required for a full understanding of the disease and for the identification of novel therapeutic targets. The late-symptomatic (P5) gene expression data presented in this study, supported by validation western blot experiments, provide some initial insights into these pathways. Whilst we cannot at this point dissect gene expression changes *causing* pathology from those *resulting from* pathological changes, nor directly measure and compare gene expression changes in vulnerable and stable populations of lower motor neurons, the data suggest that extracellular matrix integrity, growth factor signalling and myelination pathways are all significantly modified in SMA spinal cord. Moreover, the finding that gene expression changes are present in late symptomatic SMA spinal cord supports the prediction of altered gene expression based on SMN's known role in

snRNP assembly as well as studies showing that reduced snRNP assembly in the spinal cord correlates with severity of SMA disease in mice [34-37].

Whilst acknowledging the limitations of comparing gene expression on whole spinal cord extracts rather than isolated populations of lower motor neurons (which remains a technical challenge in neonatal mouse models of SMA), these microarray data represent the first attempt to understand pathways underlying pathological changes in the spinal cord in a mouse model of severe SMA. However, similar gene expression studies have previously been published using different mouse models of very mild forms of SMA [e.g. 38]. Although a comparison of the individual expression changes reported previously shows very little overlap with our experiments - as might be expected given the differing nature of pathological changes between the two models – previous studies highlighted similar changes in the expression of genes associated with the extracellular matrix [38]. It is conceivable that therapeutic strategies designed to preserve and support the extracellular matrix (often referred to as peri-neuronal nets in the nervous system) may help to sustain lower motor neuron form and function by influencing factors such as the maintenance of cellular relationships and adhesion, the control of synaptic plasticity and neurotransmitter receptor localisation, and the concentration of growth factors around neurons [39,40]. Similarly, the finding that genes associated with growth factor signalling are dys-regulated in late-symptomatic SMA spinal cord suggests that lower motor neurons may be breaking down as a result of abnormal trophic signalling. Trophic factors have long been considered as potential therapeutic agents for SMA [41], but a comprehensive analysis of the effects of different growth factors on SMA pathology has yet to be undertaken. Finally, our finding that key myelin proteins have reduced mRNA and protein levels in late-symptomatic SMA spinal cord may be of particular interest given that developmental downregulation of SMN *in vivo* coincides with the onset of

myelination [42]. Further investigations into the importance of growth factors, the extracellular matrix and myelination in SMA pathogenesis are therefore required.

In summary, we have shown that abnormal pre-symptomatic development of lower motor neuron connectivity is not a pre-requisite for subsequent neuromuscular pathology in a mouse model of severe SMA. Future experiments examining neurodevelopmental aspects of the neuromuscular system in human tissue samples will now be required to confirm the relevance of our findings for human SMA pathogenesis. Future experiments will also be required to identify molecular mechanisms underlying the triggering of neuromuscular breakdown around the time of initial symptom onset, building on our identification of changes in pathways including extracellular matrix integrity, growth factor signalling and myelination.

Materials & Methods

Mice

Smn$^{+/-}$*;SMN2* mice (Jackson labs strain no. 005024) were maintained as heterozygote breeding pairs under standard SPF conditions in animal care facilities in Edinburgh. All animal procedures and breeding were performed in accordance with Home Office and institutional guidelines. Litters produced from SMA colonies were retrospectively genotyped using standard PCR protocols (JAX® Mice Resources). *Smn-/-;SMN2;delta7* mice were maintained as heterozygote breeding pairs under standard SPF conditions in animal care facilities in Oxford. Breeding and genotyping of these mice was performed as previously described [7]. Littermate mice (*Smn*$^{+/+}$*;SMN2*) were used for controls throughout.

Immunocytochemistry

Neonatal (P1 for pre-symptomatic and P5 for late-symptomatic) *Smn-/-;SMN2* mice and

control littermates were killed by chilling on ice and decapitation. The levator auris longus (LAL), adductor auris longus (AAL) and auricularis superior (AS) muscles from the back of the neck were dissected in oxygenated mammalian physiological saline (mM: NaCl 120, Kcl 5, $CaCl_2$ 2, $MgCl_2$ 1, NaH_2PO_4 0.4, $NaHCO_3$ 23.8, D-glucose 5.6). Muscles were exposed to α-bungarotoxin (BTX) conjugated to tetramethyl-rhodamine isothiocyanate (TRITC-α-bungarotoxin; 5mg/ml, Molecular Probes) for 10 minutes and fixed in 0.1M PBS containing 4% Paraformaldehyde (Electron microscopy sciences) for 15 minutes at room temperature. Muscles were blocked in 4% bovine serum albumin (BSA) and 1% TritonX in 0.1M PBS for 30min before overnight incubation in primary antibodies raised against 150kDa neurofilament proteins (1:350 dilution; Chemicon International). After several rapid washes in 0.1M PBS, muscles were incubated in a 1:40 dilution of swine anti-rabbit secondary antibody conjugated to the fluorescent label FITC (Dako) for 4h. Muscles were whole-mounted in Mowoil® (Calbiochem) on glass slides and cover-slipped before imaging.

Imaging and analysis

Muscle preparations were viewed using either a standard epi-fluorescence microscope equipped with a chilled CCD camera (40x objective; 0.8NA; Nikon IX71 microscope; Hammamatsu C4742-95), and/or a laser scanning confocal microscope (63x objective; 1.4NA; Zeiss Axioskop). TRITC-α-BTX-labelled preparations were imaged using 543nm excitation and 590nm emission optics and FITC-labelled preparations utilised 488nm excitation and 520nm emission optics. For confocal microscopy, 488nm and 543nm laser lines were used for excitation and confocal Z-series were merged using ImageJ software. For deconvolution analysis, images were acquired using nyquist sampling and deconvolved using Huygens deconvolution software. All images were assembled for publication using Adobe Photoshop software.

Morphological Quantification and Statistics

All muscles used for quantification were imaged and reconstructed using Adobe Photoshop software so that the whole innervation pattern could be visualised, thus allowing orientation for subsequent analysis and elimination of any muscles which were damaged during dissection. All analyses were performed with the experimenter blind to genotype and muscle region. The number of endplates per axon was quantified by evaluating axon number from deconvolved images. Images were taken at approximately 100µm from the endplate area of interest to minimise variability introduced from axon branching occurring adjacent to sites of innervation. All muscles in which the complete area of innervation could not be seen, or additional axons branches were present, were excluded from further analysis. Axon numbers were counted by visualisation in the X-Y plane and scanning up and down through the z-series. This was done at three pre-defined points per image with images re-blinded between each measurement. The average of each three counts was divided by the total number of endplates innervated by the axon bundle to give the average number of axons per endplate. The average number of inputs was evaluated by counting the number of pre-synaptic inputs contacting a given endplate. Any endplate in which the complexity of innervation made it difficult to define (e.g. overlying a major nerve branch) was excluded from further analysis. Quantification was performed on a minimum of 3 images per muscle (AS,AAL) or muscle band (LAL) totalling a minimum of 15 endplates per muscle/muscle band per mouse. To quantify sprouting, sprouts were catagorised as 'small sprouts' (those less than 150µm) or 'super sprouts' (those exceeding 150µm). Sprouts were defined as a neurofilament positive process that did not project to a cluster of AChR receptors. Small sprouts were quantified by counting the number of sprouts in a given field of view expressed in relation to the number of endplates present. A minimum of three fields of view were evaluated for each muscle (AAL/AS) or muscle band (LAL). Super sprouts were quantified by counting the total

number of sprouts in a muscle region (C2 or R3-5 for LAL, whole muscle for AS/AAL) divided by the total number of endplates in the relevant region. Endplate maturation was evaluated by catagorising endplates as either uniform (even distribution of AChRs), folded (bright bands within the AChR region) or perforated (holes within the AChR staining) (see Figure 5). Any endplate which was difficult to quantify due to orientation or proximity of other endplates was excluded from further analysis. For endplate area measurements, confocal images were imported into image J software and their outline was manually traced and the software used to calculate the area. Again, any endplate which difficult to measure due to orientation or proximity of other endplates was excluded. All data were collected and analysed using GraphPad Prism software.

RNA Isolation and Microarray

Whole spinal cords were removed and RNA was extracted using an RNEasy micro kit (Qiagen). Any genomic DNA was removed using an on column digest. The quality and integrity of RNA was assessed on a BioAnalyzer; all samples had a RNA Integrity Number (RIN) ≥9 (Agilent Laboratories, US). 1µg starting RNA was ribosome depleted using the Ribominus Human/Mouse Transcriptome Isolation kit (Invitrogen). Labelled sense ssDNA for hybridization was generated with the Affymetrix GeneChip WT sense target labelling and control reagents kit (Affymetrix, UK) according to the manufacturer's instructions. Sense ssDNA was fragmented and the distribution of fragment lengths was measured on the BioAnalyser. The fragmented ssDNA was labelled and hybridized to the Affymetrix GeneChip Mouse Exon 1.0 ST Array (Affymetrix). Chips were processed on an Affymetrix GeneChip Fluidics Station 450 and Scanner 3000. The core genes on the arrays were RMA normalized in GeneSpring GX 9 and differentially expressed genes were identified using an unpaired t-test with a p-value cut off of ≤0.05 and a fold change difference between SMA and

wild-type samples of ≥1.5. No multiple testing correction was applied to the data. The genes were sorted according to their gene ontology using GenMAPP's GO-Elite. Only MAPPFinder ontologies with ≥3 genes changing and a permuted p-value ≤0.05 were selected. All array data has been submitted to MIAMExpress, where it will be publically available in ArrayExpress at The European Bioinformatics Institute (http://www.ebi.ac.uk/microarray-as/ae/).

Quantitative fluorescent western blotting

Quantitative western blots were performed as described previously [43,44], using antibodies against myelin protein P0 (Abcam, ab64685) and neuronal beta-tubulin (Abcam, ab24629) and a Typhoon laser scanner.

Acknowledgements

We thank Dr Tom Wishart, Trudi Gillespie, Derek Thomson and Laura Comley for advice and assistance with experiments. This work was supported by grants from BDF Newlife (to THG/KT); Medical Research Scotland (to THG); The Anatomical Society of Great Britain & Ireland (to LM/THG); the SMA Trust (to DB); and the Medical Research Council (to SL). We thank the Wellcome Trust Integrative Physiology Initiative in Ion Channels and Diseases of Electrically Excitable Cells (OXION) for use of the microarray facility.

Conflict of Interest Statement

The authors have no conflicts of interest to declare.

References

1. Monani, U.R. (2005) Spinal muscular atrophy: A deficiency in a ubiquitous protein; a motor neuron-specific disease. *Neuron* **48,** 885-896.

2. Pearn, J. (1978) Incidence, prevalence, and gene frequency studies of chronic childhood spinal muscular atrophy. *J. Med. Genet.* **15,** 409-413.

3. Talbot, K. and Davies, K.E. (2001) Spinal muscular atrophy. *Sem. Neurol.* **21,** 189-197.

4. Lefebvre, S., Bürglen, L., Reboullet, S., Clermont, O., Burlet, P., Viollet, L., Benichou, B., Cruaud, C., Millasseau, P., Zeviani, M., et al. (1995) Identification and characterization of spinal muscular atrophy-determining gene. *Cell* **80,** 155-165.

5. Cifuentes-Diaz, C., Nicole, S., Velasco, M.E., Borra-Cebrian, C., Panozzo, C., Frugier, T., Millet, G., Roblot, N., Joshi, V. and Melki, J. (2002) Neurofilament accumulation at the motor endplate and lack of axonal sprouting in a spinal muscular atrophy mouse model. *Hum. Mol. Genet.* **11,** 1439-1447.

6. Swoboda, K.J., Prior, T.W., Scott, C.B., McNaught, T.P., Wride, M.C., Reyna, S.P. and Bromberg, M.B. (2005) Natural history of denervation in SMA: relation to age, SMN2 copy number, and function. *Ann. Neurol*. **57,** 704-712.

7. Murray, L.M., Comley, L.H., Thomson, D., Parkinson, N., Talbot, K. and Gillingwater, T.H. (2008) Selective vulnerability of motor neurons and dissociation of pre- and post-

synaptic pathology at the neuromuscular junction in mouse models of spinal muscular atrophy. *Hum. Mol. Genet.* **17**, 949-962.

8. Kariya, S., Park, G.H., Maeno-Hikichi, Y., Leykekhman, O., Lutz, C., Arkovitz, M.S., Landmesser, L.T. and Monani, U.R. (2008) Reduced SMN protein impairs maturation of the neuromuscular junctions in mouse models of spinal muscular atrophy. *Hum. Mol. Genet.* **17**, 2552-2569.

9. Kong, L., Wang, X., Choe, D.W., Polley, M., Burnett, B.G., Bosch-Marcé, M., Griffin, J.W., Rich, M.M. and Sumner, C.J. (2009) Impaired synaptic vesicle release and immaturity of neuromuscular junctions in spinal muscular atrophy mice. *J. Neurosci.* **29**, 842-851.

10. Shafey, D., MacKenzie, A.E. and Kothary, R. (2008) Neurodevelopmental abnormalities in neurosphere-derived neural stem cells from SMN-depleted mice. *J. Neurosci. Res.* **86**, 2839-2847.

11. Rossoll, W., Jablonka, S., Andreassi, C., Kroning, A-K., Karle, K., Monani, U.R. and Sendtner, M. (2003) Smn, the spinal muscular atrophy-determining gene product, modulates axon growth and localization of β-actin mRNA in growth cones of motoneurons. *J. Cell. Biol.* **163,** 801-812.

12. Fan, L. and Simard, L.R. (2002) Survival motor neuron (SMN) protein: role in neurite outgrowth and neuromuscular maturation during neuronal differentiation and development. *Hum. Mol. Genet.* **11,** 1605-1614.

13. McWhorter, M.L., Monani, U.R., Burghes, A.H.M. and Beattie, C.E. (2003) Knockdown of the survival motor neuron (Smn) protein in zebrafish causes defects in motor axon outgrowing and pathfinding. *J. Cell Biol.* **162,** 919-931.

14. Ymlahi-Ouazzani, Q.J., Bronchain, O., Paillard, E., Ballagny, C., Chesneau, A., Jadaud, A., Mazabraud, A. and Pollet, N. (2009) Reduced levels of survival motor neuron protein leads to aberrant motoneuron growth in a Xenopus model of muscular atrophy. *Neurogenetics* In press

15. McGovern, V.L., Gavrilina, T.O., Beattie, C.E. and Burghes, A.H. (2008) Embryonic motor axon development in the severe SMA mouse. *Hum. Mol. Genet.* **17**, 2900-2909.

16. Azzouz, M., Le, T., Ralph, G.S., Walmsley, L., Monani, U.R., Lee, D.C., Wilkes, F., Mitrophanous, K.A., Kingsman, S.M., Burghes, A.H., et al. (2004) Lentivector-mediated SMN replacement in a mouse model of spinal muscular atrophy. *J. Clin. Invest.* **114**, 1726-1731.

17. Avila, A.M., Burnett, B.G., Taye, A.A., Gabanella, F., Knight, M.A., Hartenstein, P., Cizman, Z., Di Prospero, N.A., Pellizzoni, L., Fischbeck, K.H., et al. (2007) Trichostatin A increases SMN expression and survival in a mouse model of spinal muscular atrophy. *J. Clin. Invest.* **117**, 659-671.

18. Monani, U.R., Sendtner, M., Coovert, D.D., Parsons, D.W., Andreassi, C., Le, T.T., Jablonka, S., Schrank, B., Rossoll, W., Prior, T.W., et al. (2000) The human centromeric

survival motor neuron gene (SMN2) rescues embryonic lethality in Smn-/- mice and results in a mouse with spinal muscular atrophy. *Hum. Mol. Genet.* **9,** 333-339.

19. Le, T.T., Pham, L.T., Butchbach, M.E., Zhang, H.L., Monani, U.R., Coovert, D.D., Gavrilina, T.O., Xing, L., Bassell, G.J. and Burghes, A.H. (2005) SMNΔ7, the major product of the centromeric survival motor neuron (SMN2) gene, extends survival in mice with spinal muscular atrophy and associates with full-length SMN. *Hum. Mol. Genet.* **14,** 845-857.

20. Murray, L.M., Thomson, D., Conklin, A., Wishart, T.M. and Gillingwater, T.H. (2008) Loss of translation elongation factor (*eEF1A2*) expression *in vivo* differentiates between Wallerian degeneration and dying-back neuronal pathology. *J. Anat.* **213,** 633-645.

21. Monani, U.R., Pastore, M.T., Gavrilina, T.O., Jablonka, S., Le, T.T., Andreassi, C., DiCocco, J.M., Lorson, C., Androphy, E.J., Sendtner, M., et al. (2003) A transgene carrying an A2G missense mutation in the SMN gene modulates phenotypic severity in mice with severe (type I) spinal muscular atrophy. *J. Cell Biol.* **160,** 41-52.

22. Biondi, O., Grondard, C., Lécolle, S., Deforges, S., Pariset, C., Lopes, P., Cifuentes-Diaz, C., Li, H., della Gaspera, B., Chanoine, C., et al. (2008) Exercise-induced activation of NMDA receptor promotes motor unit development and survival in a type 2 spinal muscular atrophy model mouse. *J. Neurosci.* **28,** 953-962.

23. Marques, M.J., Conchello, J.A. and Lichtman, J.W. (2000) From plaque to pretzel: fold formation and acetylcholine receptor loss at the developing neuromuscular junction. *J. Neurosci.* **20,** 3663-3675.

24. Pun, S., Sigrist, M., Santos, A.F., Ruegg, M.A., Sanes, J.R., Jessell, T.M., Arber, S. and Caroni, P. (2002) An intrinsic distinction in neuromuscular junction assembly and maintenance in different skeletal muscles. *Neuron* **34,** 357-370.

25. Oprea, G.E., Kröber, S., McWhorter, M.L., Rossoll, W., Müller, S., Krawczak, M., Bassell, G.J., Beattie, C.E., and Wirth, B. (2008) Plastin 3 is a protective modifier of autosomal recessive spinal muscular atrophy. *Science* **320**, 524-527.

26. Foust, K.D., Nurre, E., Montgomery, C.L., Hernandez, A., Chan, C.M. and Kaspar, B.K. (2009) Intravascular AAV9 preferentially targets neonatal neurons and adult astrocytes. *Nat. Biotechnol.* **27,** 59-65.

27. Lim, S.R. and Hertel, K.J. (2001) Modulation of survival motor neuron pre-mRNA splicing by inhibition of alternative 3' splice site pairing. *J. Biol. Chem.* **276**, 45496-45483.

28. Madocsai, C., Lim, S.R., Geib, T., Lam, B.J. and Hertel, K.J. Correction of SMN2 Pre-mRNA splicing by antisense U7 small nuclear RNAs. *Mol. Ther.* **12**, 1013-1022.

29. Baughan, T.D., Dickson, A., Osman, E.Y. and Lorson, C.L. (2009) Delivery of bifunctional RNAs that target an intronic repressor and increase SMN levels in an animal model of spinal muscular atrophy. *Hum. Mol. Genet.* **18**, 1600-1611.

30. Ting, C.H., Lin, C.W., Wen, S.L., Hsieh-Li, H.M. and Li, H. (2007) Stat5 constitutive activation rescues defects in spinal muscular atrophy. *Hum. Mol. Genet.* **15**, 499-514.

31. Coady, T.H., Shababi, M., Tullis, G.E. and Lorson, C.L. (2007) Restoration of SMN function: delivery of a trans-splicing RNA re-directs SMN2 pre-mRNA splicing. *Mol. Ther.* **15**, 1471-1478.

32. Hua, Y., Vickers, T.A., Baker, B.F., Bennett, C.F. and Krainer, A.R. (2007) Enhancement of SMN2 exon 7 inclusion by antisense oligonucleotides targeting the exon. *PLoS Biol.* **5**: e73.

33. Baughan, T., Shababi, M., Coady, T.H., Dickson, A.M., Tullis, G.E. and Lorson, C.L. (2006) Stimulating full-length SMN2 expression by delivering bifunctional RNAs via a viral vector. *Mol. Ther.* **14**, 54-62.

34. Fischer, U., Liu, Q. and Dreyfuss, G. (1997) The SMN-SIP1 complex has an essential role in spliceosomal snRNP biogenesis. *Cell* **90,** 1023-1029.

35. Gabanella, F., Butchbach, M.E., Saieva, L., Carissimi, C., Burghes, A.H. and Pellizzoni, L. (2007) Ribonucleoprotein assembly defects correlate with spinal muscular atrophy severity and preferentially affect a subset of spliceosomal snRNPs. *PLoS One* **2,** e921.

36. Zhang, Z., Lotti, F., Dittmar, K., Younis, I., Wan, L., Kasim, M. and Dreyfuss, G. (2008) SMN deficiency causes tissue-specific perturbations in the repertoire of snRNAs and widespread defects in splicing. *Cell* **133,** 585-600.

37. Workman, E., Saieva, L., Carrel, T.L., Crawford, T.O., Liu, D., Lutz, C., Beattie, C.E., Pellizzoni, L. and Burghes, A.H. (2009) A SMN missense mutation complements SMN2 restoring snRNPs and rescuing SMA mice. *Hum. Mol. Genet.* **18,** 2215-2229.

38. Balabanian, S., Gendron, N.H. and MacKenzie, A.E. (2007) Histologic and transcriptional assessment of a mild SMA model. *Neurol. Res.* **29**, 413-424.

39. Celio, M.R., Spreafico, R., De Biasi, S. and Vitellaro-Zuccarello, L. (1998) Perineuronal nets: past and present. *Trends Neurosci.* **21,** 510-515.

40. Frischknecht, R., Heine, M., Perrais, D., Seidenbecher, C.I., Choquet, D. and Gundelfinger, E.D. (2009) Brain extracellular matrix affects AMPA receptor lateral mobility and short-term synaptic plasticity. *Nat. Neurosci.* **12,** 897-904.

41. Swoboda, K.J., Kissel, J.T., Crawford, T.O., Bromberg, M.B., Acsadi, G., D'Anjou, G., Krosschell, K.J., Reyna, S.P., Schroth, M.K., Scott, CB., et al. (2007) Perspectives on clinical trials in spinal muscular atrophy. *J. Child Neurol.* **22**, 957-966.

42. Gabanella, F., Carissimi, C., Usiello, A. and Pellizzoni, L. (2005) The activity of the spinal muscular atrophy protein is regulated during development and cellular differentiation. *Hum. Mol. Genet.* **14,** 3629-3642.

43. Wishart, T.M., Paterson, J.M., Short, D.M., Meredith, S., Robertson, K.A., Sutherland, C., Cousin, M.A., Dutia, M.B. and Gillingwater, T.H. (2007) Differential proteomics analysis of synaptic proteins identifies potential cellular targets and protein mediators of synaptic

neuroprotection conferred by the slow Wallerian degeneration (Wld^S) gene. *Mol. Cell Proteomics* **6,** 1318-1330.

44. Wishart, T.M., Pemberton, H.N., James, S.R., McCabe, C.J. and Gillingwater, T.H. (2008) Modified cell cycle status in a mouse model of altered neuronal vulnerability (slow Wallerian degeneration; Wld^S). *Genome Biol.* **9:** R101.

Figure Legends

Figure 1: Normal muscle innervation and motor neuron branching patterns in pre-symptomatic *Smn-/-;SMN2* mice. A – Montaged photo-inverted fluorescent micrographs of a 150kDa neurofilament labelled LAL muscle reveal the highly consistent innervation pattern previously reported [7]. The muscle consists of two bands: caudal, defined by blue lines and rostral, defined by red lines. Two endplate regions exist within the caudal band (C1 and C2) and 5 endplate regions exist within the rostral band (R1-5). B,C – Representative reconstructed LAL muscles from pre-symptomatic (P1) control (B) and *Smn-/-;SMN2* (C) mice. Note how the innervation patterns are indistinguishable between the two genotypes. D – Representative tracings of motor neurons innervating the caudal band of the LAL muscle in control and *Smn-/-;SMN2* mice showing similar gross morphology. E,F – Bar charts (mean ± SEM) showing no change in the number of endplates in control (+/+; black bars) compared to *Smn-/-;SMN2* (-/-; white bars) LAL muscles in regions R3-5 (E) and C2 (F) (ns - non-significant by an unpaired students t-test. n=7/8 per rostral/caudal band control, n=14/12 per rostral/caudal band *Smn-/-;SMN2*). Scale bars = 500µm.

Figure 2: Quantification of intramuscular axon numbers revealed no change in *Smn-/-;SMN2* mice. A,B - Confocal micrographs showing x/y projections of an axon bundle which represent the raw image (A) or the same image which has undergone deconvolution processing (B). C,D - Visualisation of the same images in z projection demonstrates the increased image clarity in deconvolved (D) images compared to raw images (C). For example, individual axon profiles easily identifiable in D (red arrows) are not easily distinguished in C (red arrows). E – Bar chart (mean ± SEM) revealing no significant change in the average number of endplates per axon in either region R3 or C2 of the LAL muscle between P1 *Smn-/-;SMN2* and control littermate mice (n=6/4 per rostral/caudal band control, n=9/10 per rostral/caudal band *Smn-/-;SMN2*; ns - non-significant by Kruskal-Wallis test with Dunn's post-hoc test). Scale bar = 15μm.

Figure 3: No significant change in the number of axonal inputs per endplate in *Smn-/-;SMN2* mice. A – Representative confocal micrograph of an LAL muscle from a P1 control littermate mouse, labelled with antibodies against 150kDa neurofilaments (green, upper left panel) and TRITC-α-bungarotoxin (red, lower left panel), illustrating the type of images used for the quantification of axonal inputs. Note the complexity of innervation patterns at this age and high degree of poly-neuronal innervation (i.e. multiple axons converging on a single motor endplate). B – Bar chart (mean ± SEM) showing no significant difference in the number of inputs per endplate in either the rostral or caudal band of the LAL muscle between P1 *Smn-/-;SMN2* and control littermate mice (n=6/6 per rostral/caudal band control, n=8/8 per rostral/caudal band *Smn-/-;SMN2*; ns - non-significant by ANOVA). Scale bar = 30μm.

Figure 4: Axonal sprouts were present in both rostral and caudal bands of the LAL muscle at P1, but were unchanged in *Smn-/-;SMN2* mice. A – Representative confocal micrographs from an immunohistochemically labelled LAL muscle preparations (green = 150kDa neurofilaments; red = post-synaptic acetylcholine receptors labelled with TRITC-α-bungarotoxin) showing the presence of small sprouts projecting from nerve terminals in both rostral (left) and caudal (right) muscle bands in both control (upper panels) and *Smn-/-;SMN2* (lower panels) mice at P1. Sprouts were identified as neurofilament positive projections not contacting AChR clusters (see white arrowheads). B – Bar chart (mean ± SEM) showing no change in the number of small sprouts per endplate in *Smn-/-;SMN2* mice compared to controls (n=6/6 per rostral/caudal band control, n=8/8 per rostral/caudal band *Smn-/-;SMN2*; ns - non-significant by ANOVA). Scale bar = 40μm. C – Representative confocal micrograph reconstructions showing large super sprouts (axonal projections exceeding 150um in length; white arrowheads) in rostral band regions R3-5 and caudal band region C2 from immunohistochemically labelled LAL muscle preparations from P1 control (+/+) and *Smn-/-;SMN2* (-/-) mice (green = 150kDa neurofilaments; red = post-synaptic acetylcholine receptors labelled with TRITC-α-bungarotoxin). D – Bar chart (mean ± SEM) showing no significant difference in the numbers of super sprouts (normalised to the number of endplates) present in regions R3-5 and C2 of the LAL muscle of *Smn-/-;SMN2* mice (n=8/8 per rostral/caudal band control, n=15/14 per rostral/caudal band *Smn-/-;SMN2*; ns - non-significant by ANOVA). Scale bars = 20μm.

Figure 5: AChR receptor clustering and maturation were normal in P1 *Smn-/-;SMN2* mice. A – Representative micrographs of AChRs labelled with TRITC-α-bungarotoxin showing parameters for classification of endplates as either uniform (left; even distribution of AChR receptors), folded (middle; bright bands appear representing formation of post

synaptic folds), or perforated (right; holes appear in AChR receptor clustering). B – Bar chart (mean ± SEM) showing the percentage of endplates in regions R3-5 and C2 of the LAL muscle from *Smn-/-;SMN2* (-/-) and control (+/+) mice which conform to a uniform (black bars), folded (grey bars) or perforated (white bars) morphology. No significant difference was observed between *Smn-/-;SMN2* and control animals (P>0.05; Kruskal-Wallis test) although there was an increase in endplate maturation in the caudal band compared to the rostral band, as evidenced by an increase in perforated endplates with a corresponding decrease in uniform endplates in both genotypes (n=8/8 per rostral/caudal band control, n=15/14 per rostral/caudal band *Smn-/-;SMN2*). C – Box and whisker plot showing no change in the distribution of endplate areas between rostral and caudal bands of the LAL muscle from *Smn-/-;SMN2* and control mice (P>0.05 for all comparisons, Kruskal-Wallis test; n=8/8 per rostral/caudal band control, n=15/14 per rostral/caudal band *Smn-/-;SMN2*).

Figure 6: Selective vulnerability of motor units in the slow twitch auricularis superior (AS) muscle compared to the fast twitch abductor auris longus (AAL) muscle in late-symptomatic (P5) *Smn-/-;SMN2* mice. A – Representative micrographs of AAL and AS muscles sectioned coronally and stained with antibodies against either slow myosin (upper panel) or fast myosin (lower panel). Note how the AAL muscle is composed of predominantly fast twitch fibres while the AS muscle is composed of predominantly slow twitch fibres (albeit with fast-twitch fibres also present). B – Confocal micrographs from immunohistochemically labelled AAL (left) and AS (right) muscles from P5 *Smn-/-;SMN2* mice (green = 150kDa neurofilaments; red = post-synaptic acetylcholine receptors labelled with TRITC-α-bungarotoxin) showing large numbers of denervated endplates in the AS muscles while the AAL muscle remained relatively spared. C – Bar chart (mean ± SEM) showing the percentage of fully occupied endplates from P5 *Smn-/-;SMN2* AAL and AS

muscles. Note that only 75% of endplates in the AS muscle remain fully innervated at this stage of the disease whereas nearly 100% of connections remained in the AAL muscle (* P<0.01 Mann Whitney test; n = 6/6 per AAL/AS muscle and genotype). Scale bar = 100µm (A), 15µm (B).

Figure 7: Abnormal pre-symptomatic development does not account for the selective vulnerability of motor units in slow twitch muscles. A,B – Montaged photo-inverted fluorescent micrograph reconstructions of neurofilament labelled AAL (left) and AS (right) muscles from control (A) and *Smn-/-;SMN2* (B) mice indicated that the highly consistent innervation patterns formed normally, even for motor neurons innervating the pathologically-vulnerable slow-twitch AS muscle. C,D - Bar charts (mean ± SEM) showing no significant difference in the number of endplates between control (+/+; black bars) and *Smn-/-;SMN2* (-/-; white bars) AAL or AS muscles. E - Bar chart showing the percentage of endplates in AAL and AS muscles from *Smn-/-;SMN2* (-/-) and control (+/+) mice which conform to a uniform (black bars), folded (grey bars) or perforated (white bars) morphology. No significant difference was seen between *Smn-/-;SMN2* and control animals, although there was an increase in endplate maturation in the AAL compared to AS muscle in both genotypes. F – Box and whisker plot showing no change in the distribution of endplate areas between control (+/+; black bars) and *Smn-/-;SMN2* (-/-; white bars) mice in either AAL or AS muscles (P>0.05 for all comparisons, Kruskal-Wallis test). G – Representative confocal micrographs from immunohistochemically labelled AAL/AS muscle preparations from P1 control and *Smn-/-;SMN2* mice (green = 150kDa neurofilaments; red = post-synaptic acetylcholine receptors labelled with TRITC-α-bungarotoxin) showing the presence of small sprouts projecting from nerve terminals in both AAL (left) and AS (right) muscles in all muscles examined. H – Bar chart showing no significant difference in the number of small

sprouts per endplate in *Smn-/-;SMN2* mice compared to littermate controls. I - Bar chart showing no significant difference in the number of super sprouts (normalised to the number of endplates) present in AAL and AS muscles between *Smn-/-;SMN2* mice and control controls. J - Bar chart showing no significant difference between *Smn-/-;SMN2* and control mice in the number of inputs per endplate in either the AAL or AS muscle. K – Confocal micrograph reconstructions showing large super sprouts (axonal projections exceeding 150µm in length) in immunohistochemically labelled AAL (left) and AS (right) muscle preparation from a P1 control mouse. For all experiments n=8/6 per AAL/AS muscle control, n=8/9 per AAL/AS muscle *Smn-/-;SMN2* (ns = non-significant by student t-test (A,B), Kruskal Wallis test (H,I) or ANOVA (J)). Scale bars = 500µm (A,B), 15µm (G), 20µm (K).

Figure 8: Reduction in protein expression levels of myelin protein P0 in late-symptomatic SMA mouse spinal cord. A – Representative fluorescent western blots showing expression levels of myelin protein P0 and the loading control tubulin in wild-type (+/+) and *Smn-/-;SMN2* (-/-) mouse spinal cord at post-natal day 5 (P5). B – Bar chart (mean±SEM) showing a significant reduction in myelin protein P0 expression levels in *Smn-/-;SMN2* (-/-) mouse spinal cord compared to wild-type (+/+) littermate mice at post-natal day 5 (***P<0.001; Unpaired t test; n=6 independent band measurements, N=3 mice).

Table 1: Gene expression changes >1.5 fold in pre-symptomatic (P1) *Smn-/-;SMN2* mouse spinal cord compared to litter-mate controls (all genes significantly changed P<0.05; unpaired t-test).

Gene Title	Gene Symbol	Entrez Gene ID	Cytoband	Fold change	Regulation
survival motor neuron 1	Smn1	20595	13qD1	2.7	down
olfactory receptor 1288	Olfr1288	258395	2qE3	1.6	down
developmental pluripotency associated 5A	Dppa5a	434423	5qB1	1.7	up

Table 2: Gene expression changes >1.5 fold in pre-symptomatic (P1) *Smn-/-;SMN2;delta7* mouse spinal cord compared to litter-mate controls (all genes significantly changed P<0.05; unpaired t-test).

Gene Title	Gene Symbol	Fold change	Regulation
survival motor neuron 1	Smn1	3.4	down
histone cluster 1, H1c	Hist1h1c	1.8	up
histone cluster 1, H2bc et al	Hist1h2bc	1.8	up
glycoprotein 49 A /// leukocyte immunoglobulin-like receptor, subfamily B, member 4	Gp49a /// Lilrb4	1.8	up
olfactory receptor 1393 /// olfactory receptor 1392	Olfr1393 /// Olfr1392	1.6	down
laminin, alpha 2	Lama2	1.6	up
olfactory receptor 978	Olfr978	1.6	down
kallikrein 1-related peptidase b21 et al	Klk1b21	1.6	up
polymerase (RNA) II (DNA directed) polypeptide H	Polr2h	1.6	down
ribosomal protein L14 /// RIKEN cDNA 5830454E08 gene	Rpl14 /// 5830454E08Rik	1.5	down
adrenomedullin	Adm	1.5	down

Table 3: Gene expression changes >2 fold in late-symptomatic (P5) *Smn-/-;SMN2* mouse spinal cord compared to litter-mate controls (all genes significantly changed P<0.05; unpaired t-test).

Gene Title	Gene Symbol	Entrez Gene ID	Cytoband	Fold change	Regulation
myelin protein zero	Mpz	17528	1qH3	6.5	down
decorin	Dcn	13179	10qC3	4.2	down
microfibrillar-associated protein 4	Mfap4	76293	11qB2	3.8	down
peripheral myelin protein 22	Pmp22	18858	11qB3	3.7	down
osteoglycin	Ogn	18295	13qA5	3.7	down
periostin, osteoblast specific factor	Postn	50706	3qC	3.6	down
lumican	Lum	17022	10qC3	3.5	down
survival motor neuron 1	Smn1	20595	13qD1	3.5	down
prostaglandin D2 synthase (brain)	Ptgds	19215	2qA3	3.4	down
collagen, type III, alpha 1	Col3a1	12825	1qC1.1	3.0	down
collagen, type I, alpha 1	Col1a1	12842	11qD	2.9	down
histocompatibility 2, et al	H2-T22	15039	17qB1	2.7	down
procollagen C-endopeptidase enhancer protein	Pcolce	18542	5qG2	2.7	down
ATP-binding cassette, sub-family A (ABC1), member 8a	Abca8a	217258	11qE1	2.6	down
thrombomodulin	Thbd	21824	2qG3	2.5	down
fibronectin 1	Fn1	14268	1qC3	2.5	down
reticulocalbin 3, EF-hand calcium binding domain	Rcn3	52377	7qB4	2.4	down
dipeptidylpeptidase 4	Dpp4	13482	2qC1.3	2.3	down
collagen, type I, alpha 2	Col1a2	12843	6qA1	2.3	down
asporin	Aspn	66695	13qA5	2.3	down
immunoglobulin superfamily containing leucine-rich repeat	Islr	26968	9qB	2.3	down
dermatopontin	Dpt	56429	1qH2.2	2.2	down
solute carrier family 6 (neurotransmitter transporter, GABA), member 13	Slc6a13	14412	6qF1	2.2	down
serine (or cysteine) peptidase inhibitor, clade G, member 1	Serping1	12258	2qD	2.2	down
collagen, type XII, alpha 1	Col12a1	12816	9qE1	2.2	down
gap junction protein, beta 2	Gjb2	14619	14qC3	2.2	down
cadherin 5	Cdh5	12562	8qD3	2.2	down
nidogen 2	Nid2	18074	14qA3	2.1	down
AE binding protein 1	Aebp1	11568	11qA1	2.1	down
Rho GTPase activating protein 19	Arhgap19	71085	19qC3	2.1	down
solute carrier family 7 (cationic amino acid transporter, y+ system), member 11	Slc7a11	26570	3qC	2.1	down
histone cluster 1, H2bb	Hist1h2bb	319178	13qA3.1	2.1	down
solute carrier family 13 (sodium/sulfate symporters), member 4	Slc13a4	243755	6qB1	2.1	down
vesicle-associated membrane protein 5	Vamp5	53620	6qC1	2.0	down
vitronectin	Vtn	22370	11qB5	2.0	down
insulin-like growth factor 2	Igf2	16002	7qF5	2.0	down
serine (or cysteine) peptidase inhibitor, clade D, member 1	Serpind1	15160	16qA3	2.0	down
CD93 antigen	Cd93	17064	2qG3	2.0	down
laminin, alpha 2	Lama2	16773	10qA4	2.0	down

Table 4: Pathway analysis of late-symptomatic (P5) microarray results.

GOID	GO Name	GO Type	Number Changed	Number Measured	Number in GO	Percent Changed	Percent Present	Z Score	PermuteP	Adjusted P
≥3 genes changing & ≥50% genes changing p0.05										
43256	laminin complex	C	3	5	7	60	71	12.7	0	0
48407	platelet\-derived growth factor binding	F	4	8	9	50	89	13.3	0	0
≥3 genes changing and 20-49% genes changing p0.05										
42573	retinoic acid metabolic process	P	4	10	11	40	91	11.8	0	0
5605	basal lamina	C	3	8	11	38	73	9.9	0	0
46332	SMAD binding	F	3	8	10	38	80	9.9	0	0
6776	vitamin A metabolic process	P	5	15	18	33	83	12.0	0	0
5201	extracellular matrix structural constituent	F	7	24	24	29	100	13.2	0	0
1523	retinoid metabolic process	P	3	11	14	27	79	8.3	0	0
16101	diterpenoid metabolic process	P	3	11	14	27	79	8.3	0	0
30199	collagen fibril organization	P	4	15	18	27	83	9.5	0	0
6775	fat\-soluble vitamin metabolic process	P	5	19	25	26	76	10.6	0	0
6721	terpenoid metabolic process	P	3	13	18	23	72	7.6	0	0
5520	insulin\-like growth factor binding	F	4	18	20	22	90	8.6	0	0
5581	collagen	C	4	18	19	22	95	8.6	0	0
44420	extracellular matrix part	C	13	59	71	22	83	15.5	0	0
≥3 genes changing and 10-19% genes changing p0.05										
6022	aminoglycan metabolic process	P	3	17	20	18	85	6.6	0	0
30203	glycosaminoglycan metabolic process	P	3	17	20	18	85	6.6	0	0
19838	growth factor binding	F	8	50	56	16	89	10.1	0	0
5604	basement membrane	C	7	44	54	16	81	9.5	0	0
6817	phosphate transport	P	11	70	80	16	88	11.8	0	0
30198	extracellular matrix organization and biogenesis	P	7	49	59	14	83	8.9	0	0
16620	oxidoreductase activity\, acting on the aldehyde or oxo group of donors\, NAD or NADP as acceptor	F	3	22	27	14	81	5.7	0.0005	0.0645
5578	proteinaceous extracellular matrix	C	31	234	267	13	88	18.0	0	0
31012	extracellular matrix	C	31	238	271	13	88	17.8	0	0
1871	pattern binding	F	10	79	93	13	85	9.9	0	0
5539	glycosaminoglycan binding	F	9	72	79	13	91	9.3	0	0
8201	heparin binding	F	7	56	62	13	90	8.2	0	0
30247	polysaccharide binding	F	9	76	86	12	88	9.0	0	0
6720	isoprenoid metabolic process	P	3	26	35	12	74	5.1	0.0035	0.2485
6334	nucleosome assembly	P	4	36	94	11	38	5.8	0.0005	0.0645
7160	cell\-matrix adhesion	P	8	75	85	11	88	8.0	0	0
16903	oxidoreductase activity\, acting on the aldehyde or oxo group of donors	F	3	30	36	10	83	4.7	0.0015	0.147
7422	peripheral nervous system development	P	3	30	34	10	88	4.7	0.002	0.176
1656	metanephros development	P	4	41	51	10	80	5.3	0.0005	0.0645
7596	blood coagulation	P	5	52	59	10	88	5.9	0.0005	0.0645

FIGURE 1

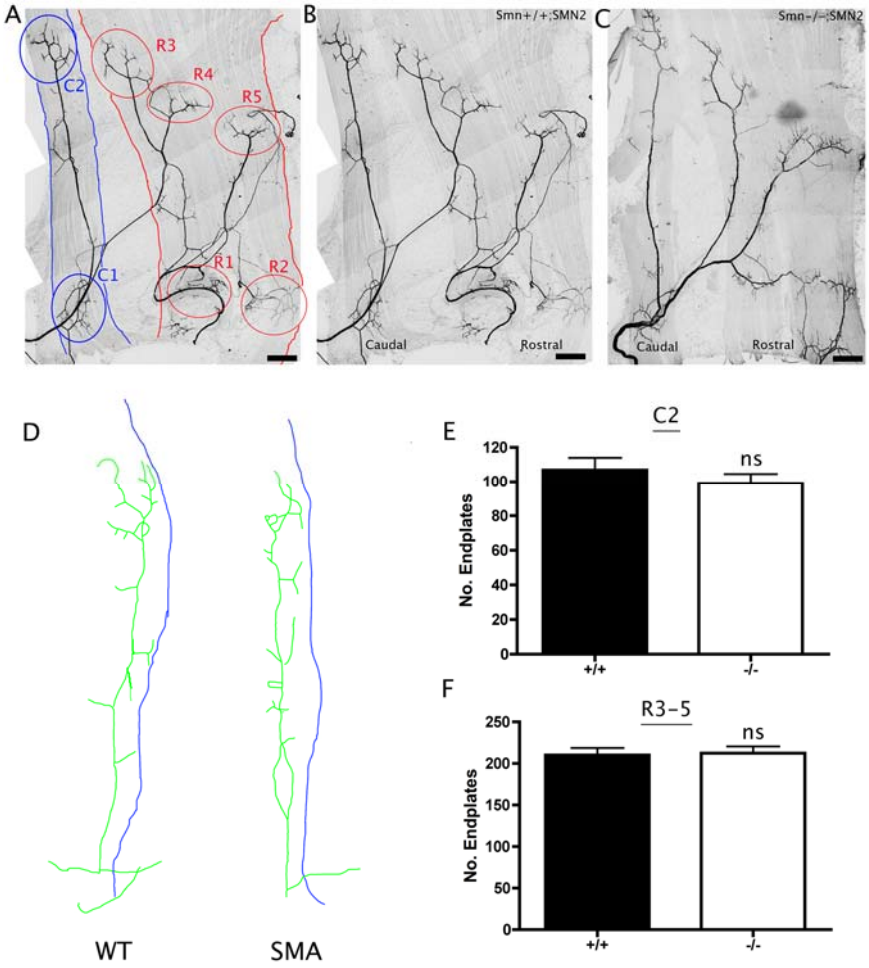

FIGURE 2

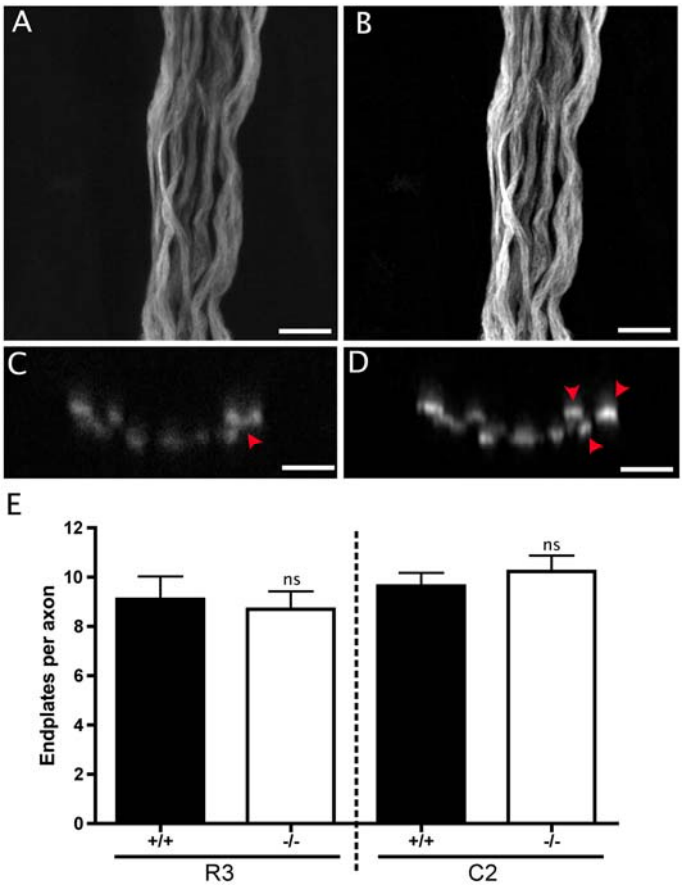

FIGURE 3

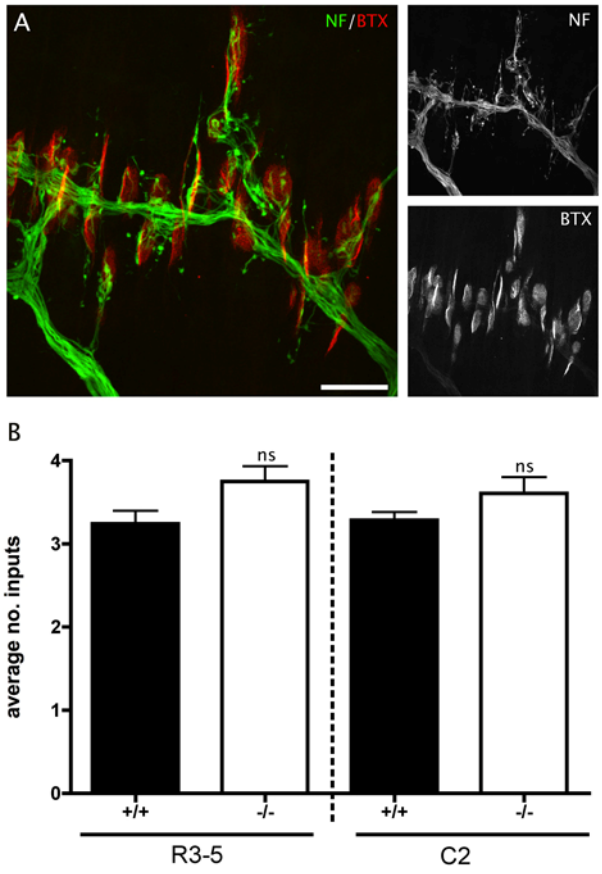

FIGURE 4

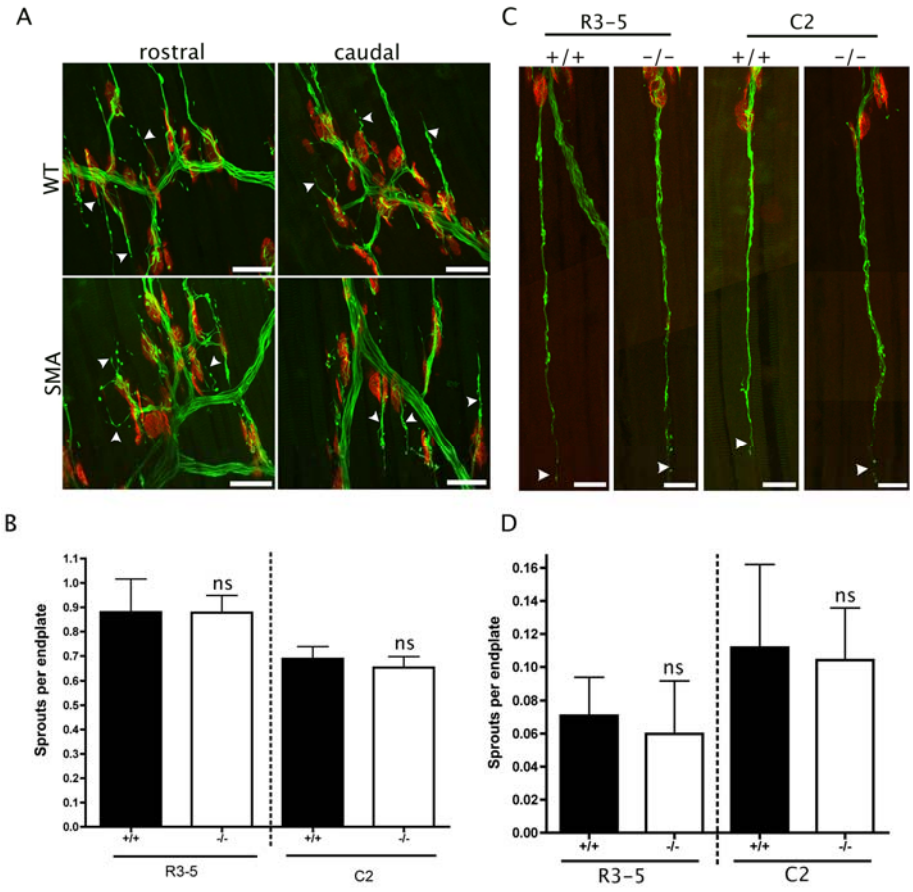

FIGURE 5

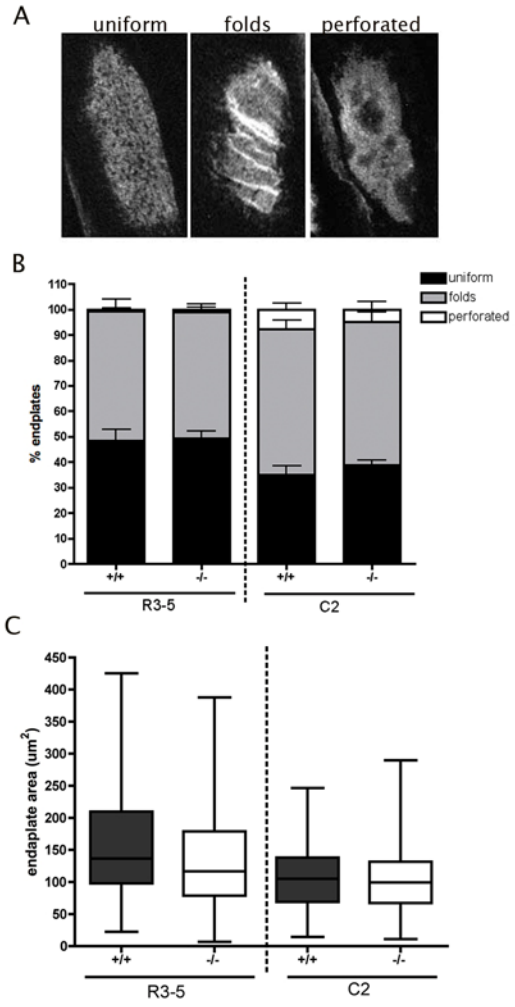

FIGURE 6

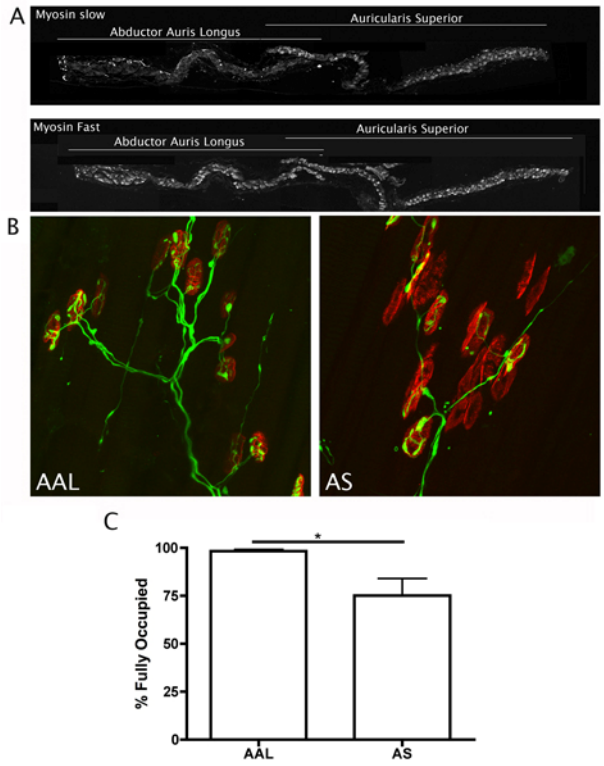

FIGURE 7

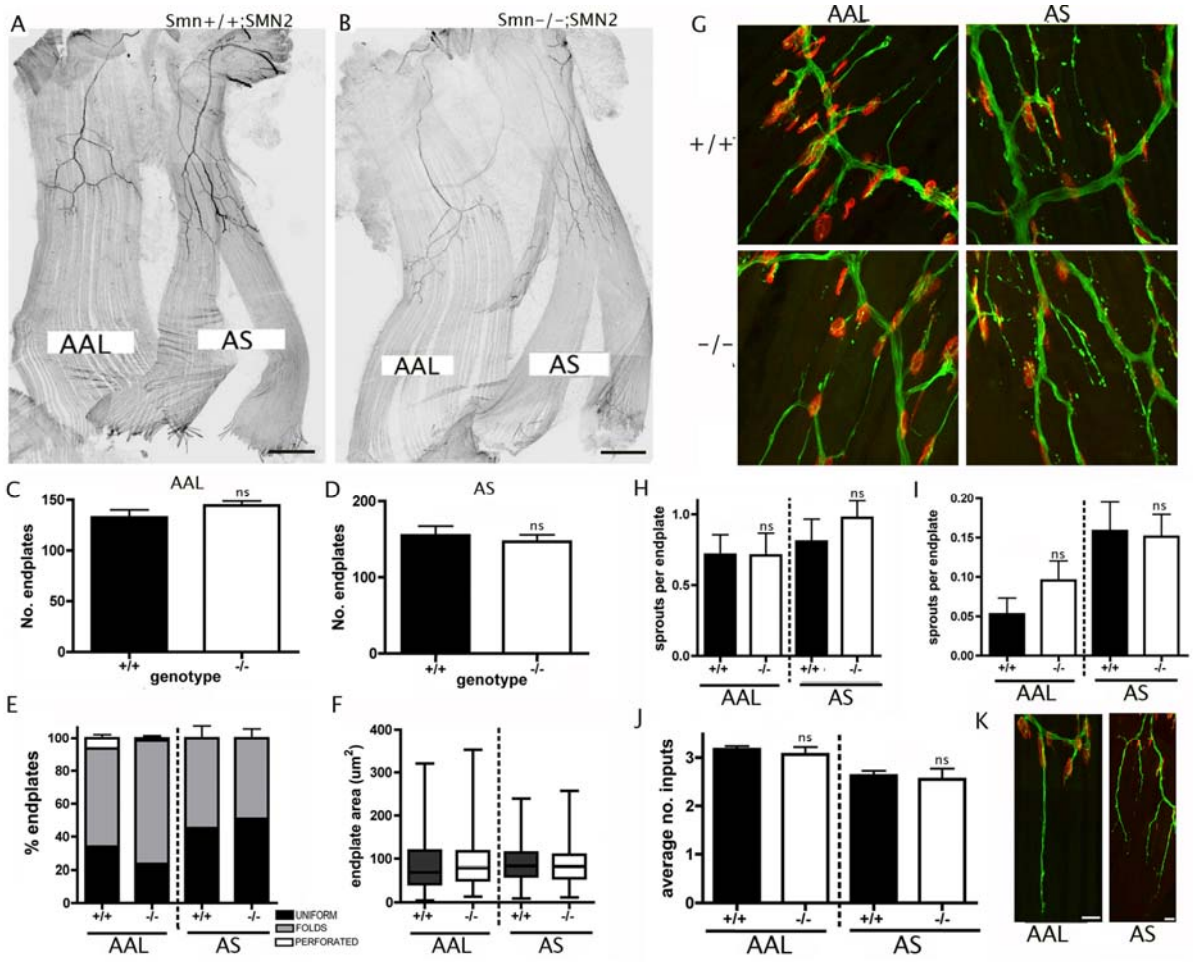

FIGURE 8

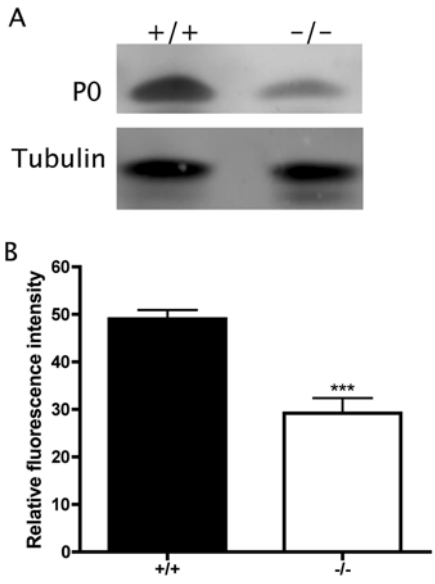

Abbreviations

AChR – Acetylcholine receptor

AAL – Abductor auris longus

AS – Auricularis superior

DeSyn – “Delayed Synapsing” neuromuscular junctions

FaSyn – “Fast Synapsing” neuromuscular junctions

LAL – Levator auris longus muscle

SMA – Spinal muscular atrophy

SMN – Survival of motor neuron gene